Published in final edited form as:
J Phys Chem C Nanomater Interfaces. 2012 December 20; 116(50): . doi:10.1021/jp306036y.

Fluorescence Intensity and Lifetime Cell Imaging with Luminescent Gold Nanoclusters

Jian Zhang[*,†], **Yi Fu**[†], **Cecil V. Conroy**[‡], **Zhenghua Tang**[‡], **Ge Li**[§], **Richard Y. Zhao**[§,‖,⊥], and **Gangli Wang**[*,‡]

[†]Center for Fluorescence Spectroscopy, University of Maryland School of Medicine, Department of Biochemistry and Molecular Biology, 725 West Lombard Street, Baltimore, Maryland 21201, United States

[‡]Department of Chemistry, Georgia State University, Atlanta, Georgia 30302, United States

[§]Division of Molecular Pathology, Department of Pathology, University of Maryland School of Medicine, 10 South Pine Street, Baltimore, Maryland 21201, United States

[‖]Department of Microbiology-Immunology, University of Maryland School of Medicine, 10 South Pine Street, Baltimore, Maryland 21201, United States

[⊥]Institute of Human Virology, University of Maryland School of Medicine, 10 South Pine Street, Baltimore, Maryland 21201, United States

Abstract

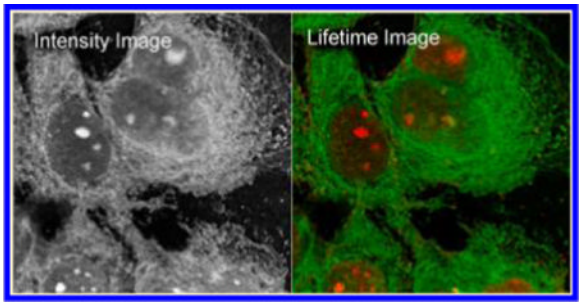

In this article, luminescent properties of gold nanoclusters (AuNCs) were studied at the single nanoparticle level and also used as novel imaging agents in cell media. Two types of water-soluble AuNCs which were stabilized with a monolayer composed of either mercaptosuccinic acid (MSA) or tiopronin thiolate ligands were synthesized by a chemical reduction reaction. These AuNCs were determined to have an average core diameter of less than 2 nm. On a time-resolved confocal microscope, the emission signals from the single AuNCs were distinctly recordable. The quantum yields of these AuNCs were measured to be ca. 5%. The lifetime of these AuNCs is also much longer than the lifetime of cellular autofluorescence in lifetime cell imaging as well as the lifetime of organic dye Alexa Fluor 488. After being derivatized with polyethylene glycol (PEG) moieties, the AuNCs were uploaded efficiently in the HeLa cells. Fluorescence intensity and lifetime cell images were recorded on the time-resolved confocal microscope in which the emission from the

[*]**Corresponding Author**jian@cfs.umaryland.eduglwang@gsu.edu. Tel.: 410-706-7500. Fax: 410-706-8408.

Supporting Information
Figures S1–S4. This material is available free of charge via the Internet at http://pubs.acs.org.

Notes
The authors declare no competing financial interest.

AuNCs was readily differentiated from the cellular autofluorescence background because of their relatively stronger emission intensities and longer lifetimes. These loaded nanoclusters in the cells were observed to widely distribute throughout the cells and especially densely loaded near the cell nucleuses. The AuNCs in the cells were also tested to have a better photostability relative to the organic fluorophores under the same conditions. We thus conclude that the AuNCs have a great potential as novel nanoparticle imaging agents, especially as lifetime imaging agents, in fluorescence imaging applications. We also prospect much broader applications of these AuNCs after further improvements of their luminescence quantum yields.

INTRODUCTION

With the advance of confocal microscopy techniques, fluorescence imaging has been widely adopted in tissue and cell studies in the past decades.[1,2] This category of techniques is now a proven powerful tool in early detection and diagnosis, guiding the treatment of diseases as well as mechanism studies in biology, immunology, and neuroscience, etc.[3–5] Among all those techniques, fluorescence lifetime imaging microscopy (FLIM) is particularly attractive[6–8] because the use of the lifetime cell imaging method can dramatically reduce the interferences from the power of excitation light source and cellular backgrounds within the cell or tissue environments in the detection of cellular processes.[9,10]

In the classic emission intensity-resolved and the newly developed lifetime-resolved fluorescence imaging measurements, the molecular imaging agents are typically needed to emit the signals that distinguish the information-of-interest from the cellular autofluorescence backgrounds in the cell images. Because the desired information strongly relies on the functions of the imaging agents, the development of new imaging agents that may display improved optical and chemical properties has attracted extensive research interest.[11,12] So far, most imaging agents are composed of conventional organic fluorophores, which can be covalently or noncovalently bound with biomarker molecules against the receptors of interest in the cells or tissues.[6] However, the organic fluorophores have significant drawbacks in the fluorescence lifetime cell imaging. First, the emission signals from most organic fluorophores overlap at least in part with cellular backgrounds. Second, the application of organic fluorophores is also compromised by their relatively low chemical and photo stability. Third, the relatively small Stokes shift between the excitation and emission complicates the imaging measurements. Finally, most organic fluorophores have their lifetimes in a range of 2–5 ns, close to the lifetime of cellular autofluorescence,[13,14] and as a result, the emission signals from them cannot be well resolved from the cellular backgrounds in lifetime cell imaging. Therefore, there is a basic need to develop new imaging agents for the emission intensity and lifetime imaging applications.[7,8]

With the developments of nanoscience and nanotechnology, luminescent nanoparticle probes become accessible as novel imaging agents.[15,16] Semiconductor quantum dots (Qdots) are especially attractive[17–19] because of their superior optical properties such as strong emission and excellent photostability.[20,21] However, Qdots have their drawbacks that are difficult to circumvent in the imaging applications. First, Qdots are composed of semiconductor materials, so the main emission originates from the band gap transitions. As a result, the emission energy or wavelength is strongly size-dependent.[22] It means that, in general, smaller sized Qdots emit the signals mostly in the visible region which is often strongly interfered with by the cellular autofluorescence in cell imaging, whereas Qdots that can emit in the near-infrared region, the spectrum window with less background interference, generally have relatively larger sizes.[23] A large dimension will impose stronger perturbations to the targets in the cells.[19,20] Second, Qdots often contain toxic core elements that are less favorable in the biomedical applications.[24] Third, Qdots have good

photostability but also display strong photoblinking that severely influences the observations of the emission signals in cell imaging.[25] While significant improvements have been achieved, it remains a challenge to circumvent these fundamental limits.

We are interested in luminescent noble metal nanoclusters and consider using them as potential substitutes of Qdots in the applications in which those Qdot limitations are significant concerns. Typically, the metal nanoclusters are fabricated to consist of gold or silver cores protected with the assembled monolayers of organic ligand compounds.[26–28] The metal cores have diameters of less than a few nanometers, rendering the overall nanocluster dimension comparable in size with biomacromolecules. Recently, the metal nanoclusters were discovered to have discrete features in the optical properties,[29,30] including near-infrared luminescence upon excitation in a wide range of wavelengths.[31,32] Importantly, the emission wavelength/energy of Au nanoclusters were observed to be largely independent of the excitation energy and significantly relaxed from the excitation in the visible range (large Stokes shift).[31–34] Moreover, as the metal core size decreases, the ratios of surface-to-core metal atoms increase leading to a significant increase of their quantum yield.[34] All these characteristics, such as the small sizes and strong emission in the near-infrared region, suggest that the nanoclusters are promising candidates as imaging agents in fluorescence cell imaging. Furthermore, rich surface chemistry also offers convenient routes for the introduction of specific probe molecules on the surfaces of metal nanoclusters.[35,36]

The optical properties of metal nanoclusters are mostly studied on ensemble spectral measurements.[31–34,37] Only a few reports focus on the optical activities from single nanoclusters.[38–40] In this work, we studied the optical properties of single AuNCs and correlated those observations with the results from the ensemble spectral measurements. Furthermore, the AuNCs are used as molecular imaging agents for fluorescence intensity and lifetime cell imaging. To improve the uploading capability of AuNCs in the cells, the AuNCs were derivatized with polyethylene glycol (PEG) moieties through surface chemical reactions.[41,42] Fluorescence intensity and lifetime imaging were performed at single cell and subcellular levels. The AuNCs were observed to efficiently disperse throughout the cells in the fluorescence cell images. The emissions from the nanocluster probes were also found to be readily distinguished from cell autofluorescence in the lifetime images.

METHODS

Chemicals

All reagents and spectroscopic grade solvents were used as received from Fisher or Sigma-Aldrich. The RC dialysis membrane (MWCO 3500 or 8000) was obtained from Spectrum Laboratories, Inc. Nanopure water (>18.0 MΩ•cm) was used in all experiments after the purification using the Millipore Milli-Q gradient system.

Preparation of AuNCs and Their Surface Functionalization

AuNCs were synthesized using a modified strategy of Brust reaction. [9,3] Two types of carboxylate-terminal ligand compounds, 2-mercaptosuccinic acid (MSA) and *N*-(2-mercapto-propionyl)glycine (tiopronin),[32] were used as ligand compounds, respectively, to assemble on the external surfaces of the Au core. Typically, $HAuCl_4 \bullet 3H_2O$ (ca. 39.4 mg, 0.1 mmol) and a type of ligand compound (for MSA, ~45.0 mg, 0.3 mmol; for tiopronin, ca. 44.2 mg, 0.3 mmol) were codissolved in 35 mL of mixed solvent (methanol: acetic acid = 6:1). After the solution turned colorless in about 30 min, $NaBH_4$ solution (ca. 38 mg, 1 mmol, dissolved in 10 mL of cold nanopure water) was added into the reaction solution with rapid stirring at 0 °C. Dark yellow solution was formed immediately. The reduction lasted

for ca. 3 h. The solvent was removed by rotary evaporation. The crude product was redispersed in 30 mL of nanopure water. The pH of the solution was adjusted to be ca. 1 with concentrated HCl. After the dialysis in nanopure water through a regenerated cellulose dialysis tube (MWCO = 3500) for 3–4 days, the product was collected and mixed with either type of thiol, respectively. The mole ratio of AuNC over thiol is ca. 1:10 during this two-day annealing process.[44] The annealing procedure is generally employed to improve the electrochemistry features (charging peak, etc.) of Au nanoclusters in previous studies. The average size is believed to be unaffected, but the monodispersity is improved based on the electrochemistry results.[44] The final products were collected after repeating the above purification steps.

To improve the uploading capability of nanocluster probes in the cells, the terminal-carboxylate moieties on AuNCs were covalently bound with polyethylene glycol (PEG) moieties via a widely used surface condensation reaction. The reaction between the amino moieties on the amine-PEG molecules and carboxylate moieties on the nanoclusters was catalyzed by 1-(3-dimethylaminopropyl)-3-ethylcarbodiimide hydrochloride (EDC) as the condensation agent. Briefly, the carboxylateterminal AuNCs (1 mg/mL, ca. $(0.5–1) \times 10^{-5}$ M) were codissolved with methoxypolyethylene glycol amine (MW 750, $(1–2) \times 10^{-5}$ M) in aqueous solution. An excess amount of EDC (1×10^{-4}M) was added in the solution at pH = 8.5. The reaction solution was stirred for an additional 24 h at room temperature. PEGylated AuNCs in solution were recovered by centrifugation at 10 000 rpm, washed with 10 mM phosphatebuffered saline (PBS) at pH = 7.4, and further purified by dialysis (MWCO 8000) against 10 mM PBS buffer solution. Representative products of the coupling reaction were characterized by H NMR and IR as shown in Figures S1 and S2 of the Supporting Information.

Cell Culture and Incubation with the PEGylated AuNCs

HeLa cells were maintained in Dulbecco's modified Eagle's medium (DMEM), supplemented with 10% fetal bovine serum (FBS), and immobilized on the glass coverslips.[45] The cell lines were fixed in 4% paraformaldehyde in 10 mM PBS buffer for 30 min at 4 °C. The fixed cell samples were incubated with 1 nM PEGylated tiopronin-AuNCs or MSA-AuNCs for 30 min and then rinsed with 10 mM PBS-Mg buffer solution. The AuNC-loaded cell samples were dried in air and stored at 4 °C for fluorescence cell imaging measurements.

Optical Spectroscopy, Imaging, and TEM Measurements

Absorption spectra were collected on a Hewlett-Packard 8453 spectrophotometer. A PerkinElmer Spectrum 100 FT-IR spectrometer was used in the infrared studies. NMR spectra were recorded with a 400 MHz Bruker spectrometer. Ensemble fluorescence spectra were recorded on a Cary Eclipse Fluorescence Spectrophotometer. Ensemble spectral lifetime measurements were carried out by single-photon counting method on a PicoQuant modular fluorescence lifetime spectrometer (Fluo Time 100) with a PicoQuant 460–480 nm LED laser as the light source.

The imaging measurements were performed on a time-resolved scanning confocal microscope (MicroTime 200, PicoQuant),[46,47] which consists of an inverted confocal microscope coupled to a high-sensitivity detection setup. A single-mode pulsed laser diode (470 nm, 100 ps, 10 MHz) was used as the excitation source. An oil immersion objective (Olympus, 100×, 1.3 NA) was used to focus the laser beam on the sample and to collect the emission from the sample. The emission signals passed a dichroic mirror and focused onto a 75 μm pinhole for spatial filtering and were recorded on a singlephoton avalanche diode (SPAD) (SPCM-AQR-14, Perkin-Elmer Inc.). A long-pass filter over 650 nm was used to

eliminate the residual excitation signals. The data were collected with a TimeHarp 200 board and stored in timetagged time-resolved mode (TTTR). Typically, the frequency of the laser source in the measurements was 10 MHz. The images of single AuNCs and cell media were recorded with the same conditions except the laser power. For the single metal nanocluster imaging, the power was 10 μW. For the cell imaging, the power was decreased to 2 μW.

For the TEM measurements, the nanoparticle samples were diluted to nanomolar concentration in water. The solutions then were cast onto the copper grids (200 mesh) with standard carbon-coated Formvar films (200–300 Å). The samples were dried in air. TEM images were taken with a side-entry Philips electron microscope at 120 keV. The distributions of nanoparticle sizes were analyzed with Scion Image Beta Release 2 on the base on at least 200 images.

RESULTS AND DISCUSSION

In this work, the gold nanoclusters (AuNCs) were synthesized in a modified Brust strategy followed by an annealing process.[11,35,44] These AuNCs were protected with the assembled monolayers of *N*-(2-mercapto-propionyl)glycine (tiopronin)[31,48] and 2-mercaptosuccinic acid (MSA), respectively, which can improve their chemical and photo stability in solution. The terminal-carboxylate groups on AuNCs also render their solubility in aqueous solution and provide reaction sites for their further functionalization.[35,36] Transmission electron microscopy (TEM) images of MSA-AuNCs and tiopronin-AuNCs were presented in the insets of Figure 1a and b, respectively. The images show relative polydispersions on the sizes with an *average* diameter of ca. 1.5 nm that is consistent with earlier reports of these materials.[43]

Before the single nanocluster analysis, AuNCs were first evaluated in the ensemble spectral measurements. In the absorption spectra, MSA-AuNCs and tiopronin-AuNCs have similar absorbance decays from high to low energy without a significant maximum (Figure 1). The disappearance of the surface plasmon band at 520 nm from the gold nanoparticles affirms their small sizes (ca. less than 2 nm).[29,30] Upon excitation in a wide range of wavelength from 350 to 550 nm, AuNCs emit luminescence at the near-infrared region, independent of the excitation wavelength.[32–34] To match the laser source equipped on the confocal microscope, we excited AuNCs at 470 nm in the following ensemble spectral studies. The excited MSA-AuNCs were shown to exhibit a broad emission band with a maximum at 785 nm. Tiopronin-AuNCs displayed an emission similar band to MSA-AuNCs. These observations were also in agreement with the results in earlier reports.[32–34] At the comparable concentrations, MSA-AuNCs and tiopronin-AuNCs are found to have similar emission intensities, corresponding to comparable quantum yields. Using Cy5.5 as a reference, the quantum yields (QYs) of both nanoclusters were tested.[12] Typically, both the nanocluster solutions were excited at 550 nm with the same excitation intensities to obtain their emission spectra. The emission spectrum of Cy5.5 solution was also obtained under the same conditions as reference. The emission bands of the nanoclusters were integrated and compared with the integrated value of Cy5.5. The QYs of nanoclusters hence were estimated to be ca. 3.4% for the MSA-AuNC and ca. 3.8% for the tiopronin-AuNC, respectively. We notice that there is only a negligible difference in the QYs between the nanoclusters, and both are significantly higher than the values in earlier reports.[31–33] Because the emission originates from energy relaxed midgap states at the Au−S interfaces, and because the annealing procedure is known to improve the monodispersity of the AuNCs without measurable changes in the average core sizes based on electrochemistry studies,[44] the differences are postulated from the optimization of Au−S surface structures. Ongoing surface characterization is beyond the scope of this paper and will be reported separately.

The luminescence properties of single AuNCs were evaluated on a time-resolved confocal microscope. The samples were created by dropcasting an aqueous solution of AuNCs at nanomolar concentration on a clean glass coverslip and air-drying.[49] In our earlier report, the metal nanoparticles that were bound with a single fluorophore were also cast on the coverslip at such a highly diluted concentration. Single-molecule detection (SMD) on the microscope showed clearly singlestep photobleaching, indicating that most metal nanoparticles were present as individuals.[50] Thus, we believe that most AuNCs in the current study were also presented as individual nanoparticles on the coverslips.

Upon the excitation with a 470 nm laser, the emission signals from individual nanoclusters were recorded through a 650 longpass filter. Representative images of AuNCs were presented in Figure 2. The distinctly bright and round emission spots in each panel correspond to individual nanoclusters. This observation reveals an exciting fact that the emissions from the single AuNCs can be clearly recorded on the confocal microscope. For each nanocluster sample, at least 50 emission spots were collected for statistic analysis of their emission properties. The histogram results were shown in Figure 3a. The average emission intensities of both AuNCs are similar to each other, in agreement with the observations on the ensemble spectral measurements.

Besides emission intensity, the lifetime of AuNCs was also collected on the time-resolved confocal microscope. The decay curves of the emission intensities were fitted with a doubleexponential function model,[12] and the histograms of average lifetimes were presented in Figure 3b. It is shown that MSA-AuNCs have an average lifetime of 13 ns, and tiopronin-AuNCs have an average lifetime of 24 ns. The lifetime of MSA-AuNCs is shorter than the lifetime of tiopronin-AuNCs, probably due to the different coating layers on their metal cores. It is worth pointing out that the detection lifetimes of nanoclusters in this study are also significantly shorter than the lifetime reported previously from the glutathiolate-stabilized AuNCs.[51] In addition to the differences in the nanocluster composition, the discrepancy was regarded to partially result from the limitation of the photon avalanche diode (PAD) detector installed on the confocal microscope. Since the PAD detector has a detection wavelength range below 800 nm, meaning that only photons below 800 nm can be counted efficiently on the confocal microscope, the measured lifetime is shorter than the real lifetime.[49] Furthermore, it is proposed by Whetten and coworkers that the AuNCs should have two emission bands originated from the hybridization of Au and S energy states. The shorter-wavelength emission (at ca. 1.8 eV) that arises from the photons at the S1 state has a relatively shorter lifetime, whereas the emission at the long-wavelength region (at ca. 1.2–1.4 eV) that arises from the photons at the T1 state has a relatively longer lifetime. In this study, the detectable photons below 800 nm should correspond to the emission component from S1 states that have the short lifetime. The lower-energy emission signals with long-component lifetime are not recorded.

To confirm the reliability of our time-resolved confocal microscope on the lifetime measurements, we also tested the lifetime of glutathione-AuNCs. It is shown that under the same conditions with the tiopronin-AuNCs and MSA-AuNCs the glutathione-AuNCs were measured to have an average lifetime of 21 ns, comparable with the lifetime of tiopronin-AuNCs and MSA-AuNCs. It indicates that the shorter lifetimes of the tiopronin-AuNCs and MSA-AuNCs in the current research are indeed due to the microscope being used. In addition, we also measured the lifetimes of tiopronin-AuNCs and MSA-AuNCs at a lower frequency of 5 MHz excitation laser and, consequently, observed a significant increase of the longlifetime component that is over 1 μs. Since there is a lack of the time-gating system on the microscope, the long-lifetime component from the AuNCs could not be recorded accurately by the SPAD detector on the microscope. Nevertheless, both nanoclusters have a longer lifetime than cellular autofluorescence (2–5 ns) as well as most organic dyes, which

promise the isolations of their emission signals from the cellular autofluorescence in lifetime cell imaging.[23]

As a comparison with the AuNCs, the organic fluorophore of Alexa Fluor 488 was also tested at the single-molecule level under the same conditions (Figure 2c). Because the visible emission from Alexa Fluor 488 is much brighter than the AuNCs under the PAD detector, a 1/20 neutral density filter was used in the measurements. The average emission intensity from the single Alexa Fluor 488 molecules is almost 10-fold greater than those from the single AuNCs (Figure 3a), indicating that the Alexa Fluor 488 molecules are much brighter than AuNCs indeed. On the other hand, the lifetime of single Alexa Fluor 488 molecules is also much shorter at 3.4 ns (Figure 3b), a typical reference value for the organic dyes.

Photostability of the imaging agents is also an important factor of concern in the imaging applications.[52] The photostability of the single MSA-AuNCs was tested by monitoring their photobleaching time profiles (Figure 4a). The emission measurement shows a slow but graduate decay over irradiation time (tens of seconds) that is presumably due to the photodegradation of the nanoclusters. A similar trend was also observed for the tiopronin-AuNCs (not shown). In comparison, the emission time-trace measurements from the single Alexa Fluor 488 molecules show a single-step photobleaching which is a typical feature of single organic fluorophores (Figure 4b). The bleaching time of Alexa Fluor 488 molecules is less that 0.2 s, much shorter than the time of the AuNCs under the same conditions, indicating that AuNCs are at least 1000-fold more photostable over the organic fluorophores.

According to earlier reports, the PEGlyation on the nanoparticle probes can drastically improve their capability of uploading in the cell lines.[41,42] Thus, in this study, we covalently bound the PEG moieties on AuNCs via wellestablished coupling reactions on the AuNC surfaces. The terminal carboxylate groups on the AuNCs were reacted with the terminal amino groups on the PEG compounds in the presence of 1-(3-dimethylaminopropyl)-3-ethylcarbodiimide hydrochloride (EDC) as condensation agents.[35,36] To avoid a large increase in overall dimension, the AuNCs used for cell imaging were synthesized at a relatively low mole ratio of ca. 1:2 for AuNC over PEG during the coupling reaction. Due to the unknown number of (CH_2CH_2O) units per PEG molecule (average M.W. 750D), a quantification of the amount of PEG ligands per nanoclusters could not be determined. The representative NMR and IR spectra of the PEGylated AuNCs are included in Figure S1 (Supporting Information), in which the additional amide bond signatures and PEG proton signals can be clearly identified. The efficacy of the PEGylation reaction on the AuNCs was also confirmed by the change in the solubility of nanoclusters before and after the reaction. Prior to the reaction the AuNCs were found to be well soluble in water but slightly dissolved in methanol, whereas after the reaction the AuNCs became completely soluble in both water and methanol. Because the coupling reaction happens only at the ligand terminal groups, the ensemble absorbance and emission spectra of the AuNCs remain unchanged upon PEGylation. The TEM analysis of the PEGlyated AuNCs confirms the products as individuals rather than aggregates and also maintains the original core size distributions. The results demonstrate that the physical properties of the AuNCs are not significantly changed with the coupling reaction on the surfaces, in agreement with the literature.[53]

In the next study, the nanoclusters were uploaded into the HeLa cells to explore their emission properties on the fluorescence intensity and lifetime cell images. Typically, the HeLa cells fixed on the coverslips were incubated with the PEGylated MSA-AuNCs and tiopronin-AuNCs, respectively. The incubation time was ca. 30 min, which is a typical duration period for a small molecule imaging agent rather than a larger nanoparticle agent.

After washing with 10 mM PBS buffer solution, the fluorescence intensity and lifetime cell images were recorded on the time-resolved confocal microscope (Figure 5). As a negative control, the images of the blank cells without any labeling treatment were also recorded. It is obvious that the emission intensity images from the AuNC-loaded cells are much brighter than those from the blank cells, confirming uptakes of AuNCs into the cells. The overall brightness of the MSA-AuNC loaded cell images is also observed to be brighter than that with the tiopronin-AuNCs, probably because there are more MSA-AuNC uptakes in the cells under the same conditions. To evaluate the efficacy of the nanoclusters in cell imaging, the HeLa cells were also incubated with the Alexa Fluor 488 fluorophores. The emission intensity and lifetime cell images were presented in Figure 6 as respective references. Compared with the cell images with the AuNC uptakes, the cell images with the Alexa Fluor 488 dyes are much brighter due to stronger visible emission from the organic dyes and better signal responses from the PAD detector.

The AuNCs are supposed to display superior advantages over the organic fluorophores in the lifetime cell images rather than in the intensity cell images because of their relatively longer lifetimes than the lifetime of cellular autofluorescence. Thus, the lifetime cell images were also collected on the timeresolved confocal microscope (Figure 5). In comparison with the images of blank cells, the lifetime images from the AuNC-loaded cells are shown to have significantly longer lifetime components. As a result, the emission signals from the uploaded nanoclusters can be clearly distinguished from the cellular backgrounds in the lifetime cell images. In contrast, the lifetime emission signals from the Alexa Fluor 488 molecules in the cells are similar to the cellular autofluorescence with minor differences because of their comparable lifetimes. Therefore, the emissions from the organic fluorophores are almost indistinguishable from the cellular backgrounds in the lifetime cell images (Figure S3, Supporting Information).

We also notice that in the lifetime cell images the emission signals from the AuNCs are widely and heterogeneously dispersed throughout the cell images, indicating that, like the organic fluorophores, the molecular-sized AuNCs can penetrate the cell plasma membranes and access various subcellular domains during a relatively short incubation time. It is very interesting to notice that the AuNCs appear to be accumulated in the areas close to the cell nucleuses. Recent literature shows that different types of Au nanomaterials could enter the cell nucleus under different mechanisms.[54,55] Because the pores on the nuclear membrane have an average diameter of ca. 30 nm whereas the overall dimension of AuNCs is less than 5 nm, we believe that AuNCs have a high possibility to enter and accumulate in the cell nucleus.

The Z-stack images from the MSA-AuNC loaded cells are shown in Figure 6. The first image was recorded with the laser beam focused on the glass coverslip surface. In the following images, the focus was adjusted at every 1 μm away from the coverslip surface up to different layers of cells. The images from the surrounding became blurry due to the change of focus plane. Meanwhile, the signals from the nucleus region remained consistent, and the intensity inside the nucleus appeared to be heterogeneously distributed. This suggests that a sufficient amount of AuNCs are encapsulated in the cell nucleus rather than around it. Beyond 7 μm, the images from the cell nucleus also became blurry, corresponding to out of focus. Overall, the locations of those emission spots appeared to be random at different focus depths, further attesting to the penetration and actual localizations of the AuNCs in the cell and cell nucleus.

The emission signals from the AuNCs in the cytosol or plasma membrane are relatively weaker than those in the cell nucleus. It is because most nonspecifically confined AuNCs in the cytosol or plasma membrane were washed away from the fixed HeLa cells in the

treatment. The AuNCs in the nucleus are less affected because of the confinement in the nucleus. These observations are exciting in that the nanoparticle-based nucleus staining is still a technical challenge in the cell imaging applications. We expect that the use of the current nanoclusters can potentially solve this problem to some extent.

The overall emission properties over the entire cell images were obtained from the statistical analysis of the emission intensity and lifetime.[56] A minimum of 20 cell images were analyzed, and the distributions of the emission intensity and lifetime over the cell images are presented in Figure 7. The maximum of emission intensity over the images of the unlabeled cell is ca. 110 counts, which is used as a reference corresponding to the cellular autofluorescence (Figure 7a). For the images from the nanocluster-loaded cells, the maximum of emission intensity is ca. 280 counts for the tiopronin-AuNC loaded cells and 430 counts for the MSA-AuNC loaded cells. Both are significantly higher than the reference cells due to the uptakes of the nanoclusters in the cells. The cell images labeled by the Alexa Fluor 488 were also analyzed, showing a maximum of emission intensity at 410 counts. This value is also greater than the emission intensity from the cellular autofluorescence, demonstrating the uptakes of the organic dyes in the cells. Since the overall emission intensity in the cell images is closely related with the uptake amounts of nanocluster or organic dye probes within the cells, the maximal emission intensities over the cell images with the nanocluster uptakes cannot be simply compared to each other as well as that over the cell images with the organic dye uptakes.

In contrast, the lifetime images of cells are independent of uptake amount of imaging agents. In the current study, like the emission intensity over the cell images, the lifetime cell images are also analyzed to achieve their distributions over the images (Figure 7b). The results show that the unlabeled cell images have a maximum at 3 ns, corresponding to the cellular autofluorescence. The distribution curves over the AuNC-loaded cell images become much broader due to the longerlifetime component from the AuNCs uploaded in the cells. In addition, we also notice that the distribution curves from the nanocluster-loaded cell images are almost not overlapped with the blank cell ones which is significant because the emission signals from the AuNCs can be readily isolated from the cellular backgrounds in lifetime cell imaging. In comparison, the lifetime over the images of the Alexa Fluor 488-labeled cells has a maximum at 3.2 ns (Figure 6b), and the curve is significantly overlapped with the lifetime curve of cellular autofluorescence. As a result, the emissions from the Alexa Fluor 488 cannot be distinctly identified from the cellular backgrounds in lifetime cell imaging.

It is also noticed that the distribution curves of lifetime over the AuNC-loaded cell images exhibit double maxima which are 10.5 and 16.2 ns for the tiopronin-AuNC loaded cell images and 4.7 and 8.9 ns for the MSA-AuNC loaded cell images. These lifetime maxima over the lifetime cell images are significantly shorter than the lifetime maxima achieved from the single nanocluster measurements (Figure 3b), suggesting the presence of significant interference with the cellular media. The double lifetime maxima could also reflect the heterogeneous distributions of the nanoclusters throughout the cells. Actually, the lifetime parameters in the cell images are basically constituted of the emissions from the imaging agents in the cells and the autofluorescence from the cellular media and water. The nanoclusters loosely distributed in the cells will be more exposed to many potential quenching processes for the excited surface states. Consequently, the apparent lifetime maximum is shorter than that measured at more confined nucleus regions or solid states.

In this study, we also explored the photostability of the AuNCs in fluorescence cell imaging. Some emission spots were randomly selected and continuously irradiated with a 470 nm laser. The emission time profiles were collected (Figure S4, Supporting Information), showing decay from high to low intensity over time for both the nanocluster-loaded cells

and the organic dye labeled cells. This observation is consistent with the single nanocluster analysis (Figure 4), indicating that the emission spots in the images were derived from the AuNCs or organic fluorophores, either as individuals or as aggregates. It is also noticed that the emission spots on the organic dye labeled cell images are completely bleached within 5 s, whereas the emission spots on the nanocluster-loaded cell images are reduced only to about one-half over 60 s under the same conditions, suggesting that the nanoclusters have at least 20fold extensive photostability relative to the Alexa Fluor 488 dyes in the cell media.

CONCLUSIONS

Luminescent Au nanoclusters (AuNCs) are prepared and evaluated as imaging agents for fluorescence intensity and lifetime cell imaging. Upon excitation at a wide visible range, the molecular-sized AuNCs display strong emission signals in the near-infrared region and long lifetimes relative to the organic fluorophores. The emission profiles from the single AuNCs were monitored for the first time under a time-resolved confocal microscope. AuNCs were PEGlyated through the surface reactions to improve their uptake capabilities in the cells. The PEGlyated AuNCs were shown to enable efficient uploading and distribution in the HeLa cells after a short incubation. Fluorescence intensity and lifetime images were recoded at the single cell and subcellular level. With advantages of longer lifetimes from AuNCs, the emission signals from uploaded AuNCs in the cells could be easily isolated from the cellular autofluorescence backgrounds in the lifetime cell images. AuNCs were also observed to distribute throughout the cells and, interestingly, accumulate in the areas close to the cell nucleuses. Moreover, relative to the organic fluorophores of Alexa Fluor 488, the AuNCs display better photostability in cell imaging. With the low or nontoxic components (noble Au cores and amino acid-like coating layers), small dimension for the distribution to subcellular domains, versatile surface chemistry for specific targeting (biomarker oriented), wide range for excitation wavelength, near-infrared emission, and longer lifetime than autofluorescence, we believe these luminescent AuNCs have great potentials in fluorescence cell imaging applications.

Supplementary Material

Refer to Web version on PubMed Central for supplementary material.

Acknowledgments

The authors would like to thank support by grants from NIH (EB009509, HG-002655, HG005090, EB006521, and CA134386). G.W. acknowledges the financial support from NSF CHE 1059022. Z.T. acknowledges the fellowship from the Center of Diagnostics and Therapeutics (CDT) at Department of Chemistry, Georgia State University.

References

1. Ntziachristos V, Chance B. Breast Cancer Res. 2001; 3:41–46. [PubMed: 11250744]
2. Hawrysz DJ, Sevick-Muraca EM. Neoplasia. 2000; 2:388–417. [PubMed: 11191107]
3. Kobayashi H, Ogawa M, Alford R, Choyke PL, Urano Y. Chem Rev. 2010; 110:2620–40. [PubMed: 20000749]
4. Smiley RDG, Hammes G. Chem Rev. 2006; 106:3080–3094. [PubMed: 16895319]
5. Michalet X, Weiss S, Jager M. Chem Rev. 2006; 106:1785–1813. [PubMed: 16683755]
6. Kobayashi H, Choyke PL. Acc Chem Res. 2011; 44:83–90. [PubMed: 21062101]
7. Willets KA, Nishimura SY, Schuck PJ, Twieg RJ, Moerner WE. Acc Chem Res. 2005; 38:549–556. [PubMed: 16028889]
8. Thoumine O, Ewers H, Heine M, Groc L, Frischknecht R, Giannone G, Poujol C, Legros P, Lounis B, Cognet L, Choquet D. Chem Rev. 2008; 108:1565–1587. [PubMed: 18447398]

9. Berezin MY, Achilefu S. Chem Rev. 2010; 110:2641–2684. [PubMed: 20356094]
10. Lakowicz, JR. Principles of Fluorescence Spectroscopy. 3. Springer Published; New York: 2006. p. 623-672.
11. Brinkley MA. Bioconjugate Chem. 1992; 3:2–13.
12. Licha K, Riefke B, Ntziachristos V, Becker A, Chance B, Semmler W. Photochem Photobiol. 2000; 72:392–398. [PubMed: 10989611]
13. Kim HM, Cho BR. Acc Chem Res. 2009; 42:863–872. [PubMed: 19334716]
14. Knemeyer J-P, Herten D-P, Sauer M. Anal Chem. 2003; 75:2147–2153. [PubMed: 12720354]
15. Bardhan R, Lal S, Joshi A, Halas NJ. Acc Chem Res. 2011; 44:936–946. [PubMed: 21612199]
16. Louie A. Chem Rev. 2010; 110:3146–3195. [PubMed: 20225900]
17. Nozik AJ, Beard MC, Luther JM, Law M, Ellingson RJ, Johnson JC. Chem Rev. 2010; 110:6873–6890. [PubMed: 20945911]
18. Yarkony DR. Chem Rev. 2012; 112:481–498. [PubMed: 22050109]
19. Sapsford KE, Tyner KM, Dair BJ, Deschamps JR, Medintz IL. Anal Chem. 2011; 83:4453–4488. [PubMed: 21545140]
20. Kim J, Wong CY, Scholes GD. Acc Chem Res. 2009; 42:1037–1046. [PubMed: 19425542]
21. Michalet X, Pinaud FF, Bentolila LA, Tsay JM, Doose S, Li JJ, Sundaresan G, Wu AM, Gambhir SS, Weiss S. Science. 2005; 307:538–544. [PubMed: 15681376]
22. Peng X. Acc Chem Res. 2010; 43:1387–1395. [PubMed: 20695433]
23. Mahmood U, Weissleder R. Mol Cancer Ther. 2003; 2:489–496. [PubMed: 12748311]
24. Smith AM, Nie S. Nat Biotechnol. 2009; 27:732–733. [PubMed: 19668181]
25. Smith AM, Duan H, Mohs AM, Nie S. Adv Drug Delivery Rev. 2008; 60:1226–1240.
26. Jadzinsky PD, Calero G, Ackerson CJ, Bushnell DA, Kornberg RD. Science. 2007; 318:430–433. [PubMed: 17947577]
27. Zheng J, Nicovich PR, Dickson RM. Annu Rev Phys Chem. 2007; 58:409–432. [PubMed: 17105412]
28. Murray RW. Chem Rev. 2008; 108:2688–2720. [PubMed: 18558753]
29. (a) Pei Y, Zeng XC. Nanoscale. 2012; 4:4054–4072. [PubMed: 22635136] (b) Walter M, Akola J, Lopez-Acevedo O, Jadzinsky PD, Calero G, Ackerson CJ, Whetten RL, Gronbeck H, Hakkinen H. Proc Natl Acad Sci. 2008; 105:9157–9162. [PubMed: 18599443]
30. (a) Tang Z, Xu B, Wu B, Germann MW, Wang G. J Am Chem Soc. 2010; 132:3367–3374. [PubMed: 20158181] (b) Varnavski O, Ramakrishna G, Kim J, Lee D, Goodson T. J Am Chem Soc. 2009; 132(1):16–17. [PubMed: 20000663] (b) Zhu M, Aikens CM, Hollander FJ, Schatz GC, Jin R. J Am Chem Soc. 2008; 130:5883–5885. [PubMed: 18407639]
31. Zheng J, Zhou C, Yu MX, Liu JB. Nanoscale. 2012; 4(14):4073–4083. [PubMed: 22706895]
32. Huang T, Murray RW. J Phys Chem B. 2001; 105:12498–12502.
33. (a) Tang Z, Ahuja T, Wang S, Wang G. Nanoscale. 2012; 4(14):4119–4124. [PubMed: 22643767] (b) Tang Z, Xu B, Wu B, Robinson DA, Bokossa N, Wang G. Langmuir. 2011; 27:2989–2996.
34. (a) Wang G, Huang T, Murray R, Menard L, Nuzzo RG. J Am Chem Soc. 2005; 127:812–813. [PubMed: 15656600] (b) Wang G, Guo R, Kalyuzhny G, Choi JP, Murray RW. J Phys Chem B. 2006; 110:20282–20289. [PubMed: 17034208]
35. Templeton AC, Wuelfing WP, Murray RW. Acc Chem Res. 2000; 33:27–36. [PubMed: 10639073]
36. Rosi NL, Mirkin CA. Chem Rev. 2005; 105:1547–1562. [PubMed: 15826019]
37. Rycenga M, Cobley CM, Zeng J, Li W, Moran CH, Zhang Q, Qin D, Xia Y. Chem Rev. 2011; 111:3669–3712. [PubMed: 21395318]
38. Zhang J, Fu Y, Lakowicz JR. Opt Express. 2007; 15:13415–13420. [PubMed: 19550610]
39. Wang H-H, Lin C-AnJ, Lee C-H, Lin Y-C, Tseng Y-M, Hsieh C-L, Chen C-H, Tsai C-H, Hsieh C-T, Shen J-L, Chan W-H, Chang WH, Yeh H-I. ACS Nano. 2011; 5:4337–4344. [PubMed: 21608984]
40. Lin C-AJ, Yang T-Y, Lee C-H, Huang SH, Sperling RA, Zanella M, Li JK, Shen J-L, Wang H-H, Yeh H-I, Parak WJ, Chang WH. ACS Nano. 2009; 3:395–401. [PubMed: 19236077]

41. Riley T, Govender T, Stolnik S, Xiong CD, Garnett MC, Illum L, Davis SS. Colloids Surf., B. 1999; 16:147–159.
42. Endres TK, Beck-Broichsitter M, Samsonova O, Renette T, Kissel TH. Biomaterials. 2011; 32:7721–7731. [PubMed: 21782238]
43. Zhu T, Vasilev K, Kreiter M, Mittler S, Knoll W. Langmuir. 2003; 19:9518–9525.
44. Hicks JF, Miles DT, Murray RW. J Am Chem Soc. 2002; 124:13322–13328. [PubMed: 12405861]
45. Zhang J, Fu Y, Li G, Nowaczyk K, Zhao RY, Lakowicz JR. Biochem Biophys Res Commun. 2010; 400:111–116. [PubMed: 20705055]
46. Zhang J, Fu Y, Liang D, Nowaczyk K, Zhao RY, Lakowicz JR. Nano Lett. 2008; 8:1179–1186. [PubMed: 18341300]
47. Zhang J, Fu Y, Mei Y, Jiang F, Lakowicz JR. Anal Chem. 2010; 82:4464–4471. [PubMed: 20433154]
48. Zhang J, Fu Y, Lakowicz JR. J Phys Chem C. 2011; 115:7202–7208.
49. Huang T, Murray RW. J Phys Chem B. 2003; 107:7434–7440.
50. Zhang J, Fu Y, Chowdhury MH, Lakowicz JR. J Phys Chem C. 2008; 112:18–26.
51. Link S, Beeby A, FitzGerald S, El-Sayed MA, Schaaff TG, Whetten RL. J Phys Chem B. 2002; 106:3410–3415.
52. Zhang J, Fu Y, Lakowicz JR. Langmuir. 2008; 24:3429–3433. [PubMed: 18278953]
53. Zhang J, Lakowicz JR. J Phys Chem B. 2005; 109:8701–8706. [PubMed: 16852030]
54. Dam DHM, Lee JH, Sisco PN, Co DT, Zhang M, Wasielewski MR, Odom TW. ACS Nano. 2012; 6:3318–3326. [PubMed: 22424173]
55. Duan H, Nie S. J Am Chem Soc. 2007; 129:3333–3338. [PubMed: 17319667]
56. Zhang J, Fu Y, Xu X, Lakowicz JR. J Biomed Opt. 2011; 16:116004. [PubMed: 22112109]

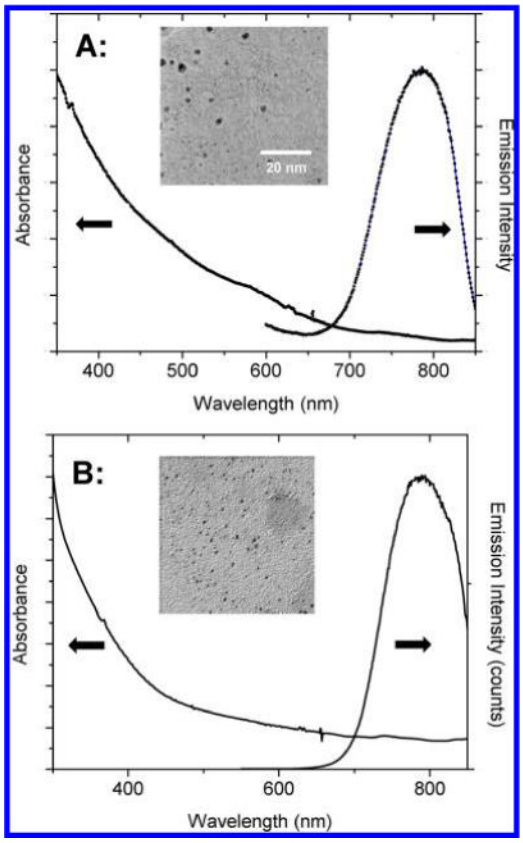

Figure 1.
Ensemble absorbance and luminescence spectra of (a) MSA-AuNCs and (b) tiopronin-AuNCs in 10 mM PBS buffer solution at pH = 7.4. Luminescence spectrum was collected upon excitation at 470 nm. The inset is a respective transmission electron micrograph (TEM) image of (a) MSA-AuNCs and (b) tiopronin-AuNCs.

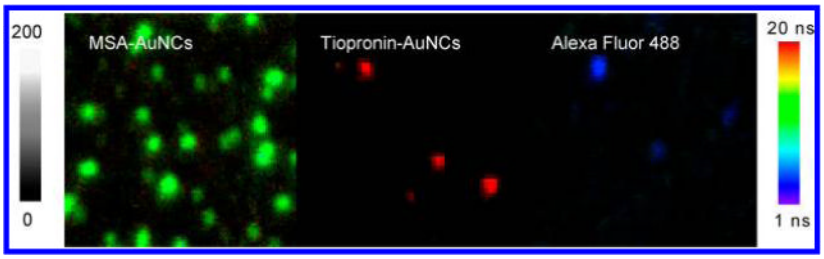

Figure 2.

Fluorescence intensity/lifetime images of single MSA-AuNCs, tiopronin-AuNCs. Fluorescence intensity/lifetime image of single Alexa Fluor 488 fluorophores was also recorded with a 1/20 neutral density filter as reference. The scales of the diagrams were 5 × 5 μm, and the resolutions of the diagrams were 100 × 100 pixels with an integration of 0.6 ms/pixel.

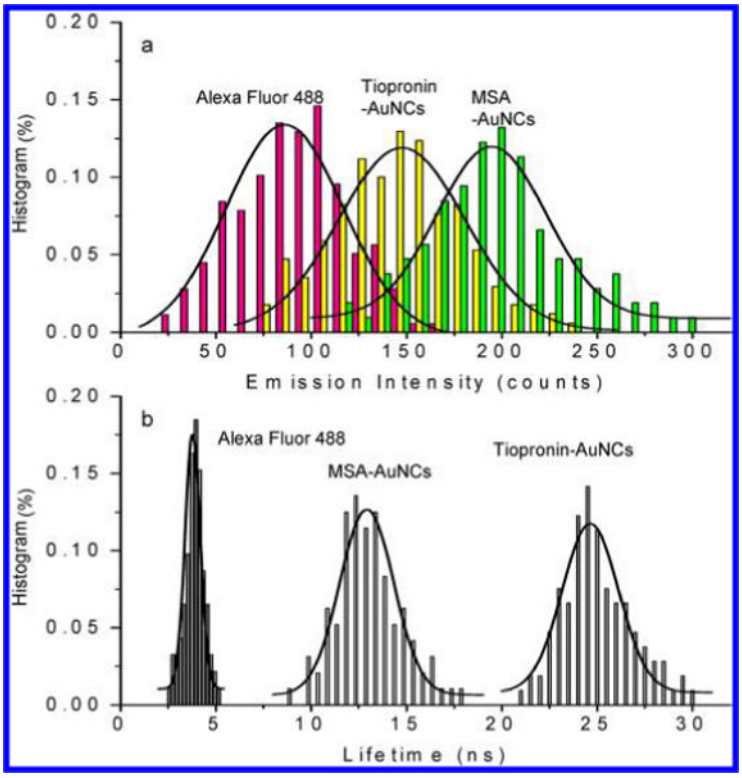

Figure 3.
Histograms of (a) emission intensities and (b) lifetimes of MSA-AuNCs and tiopronin-AuNCs. The emission intensity and lifetime data from Alexa Fluor 488 fluorophores were also collected, and the histograms were presented as controls.

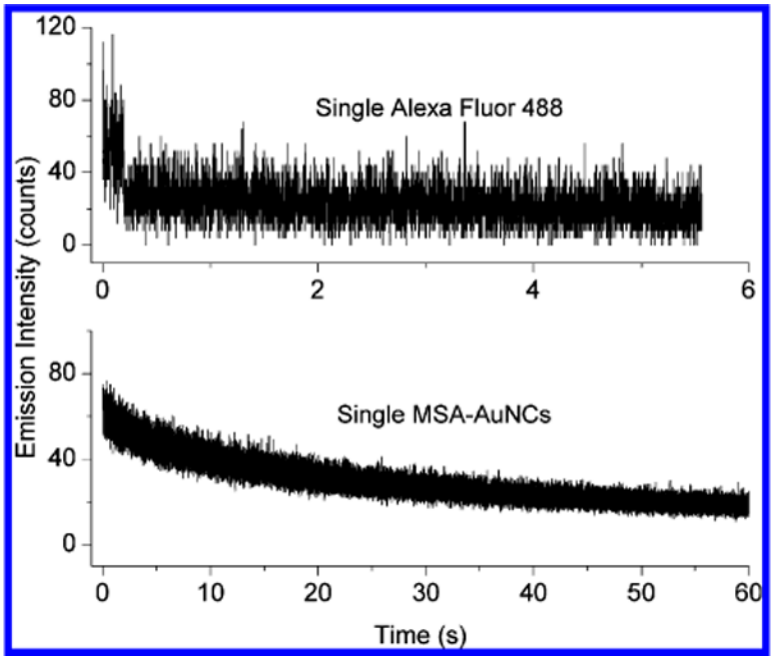

Figure 4.

(a) Representative time trace of a single MSA-AuNC displaying a slow decay with the irradiation time under a 470 nm laser irradiation. (b) A representative time trace of a single Alexa Fluor 488 fluorophore displaying a typical single-step bleaching with the irradiation time.

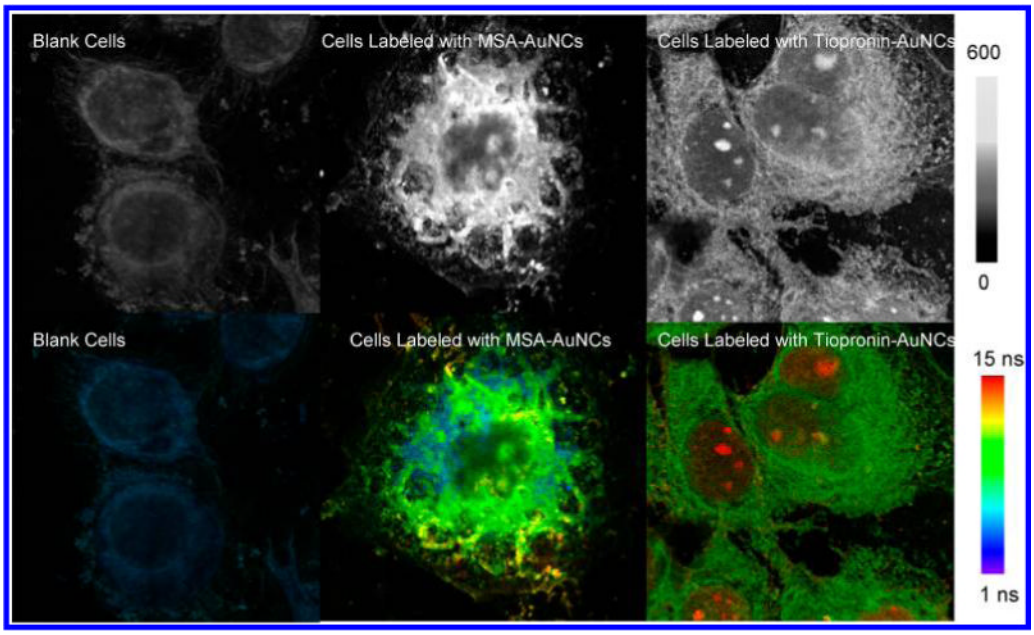

Figure 5.

Fluorescence intensity (upper panel) and lifetime (bottom panel) images of HeLa cells loaded with PEGylated MSA-AuNCs and PEGylated tiopronin-AuNCs, respectively. The cell images were collected from the emission through a 650 nm long-pass filter upon excitation at 470 nm. Fluorescence intensity and lifetime images of blank cells without labeling were also recorded under the same conditions as control. The scales of the diagrams were 80 × 80 μm, and the resolutions of diagrams were 400 × 400 pixels with an integration of 0.6 ms/pixel.

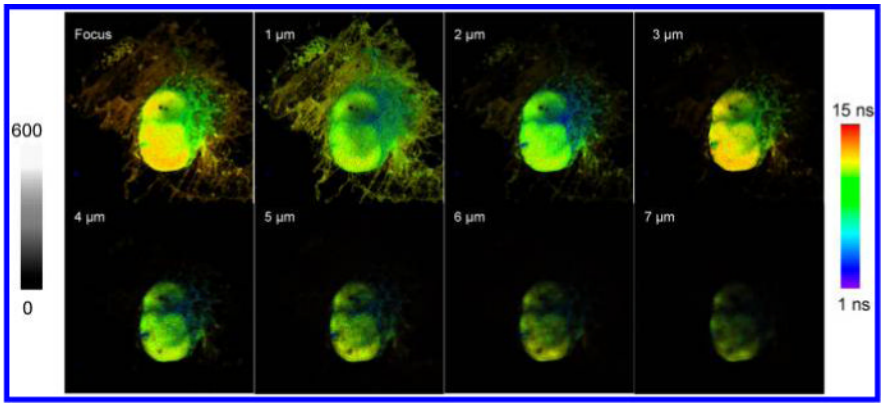

Figure 6.

Fluorescence lifetime images of HeLa cells labeled with PEGylated MSA-AuNCs. The images were collected from the emission through a 650 = long-pass filter upon excitation at 470 nm. The cells were scanned with a focus lifting from the top of the coverslip to different layers of the cell in a scale of 1 μm. The scales of the diagrams were 80 × 80 μm, and the resolutions of diagrams were 400 × 400 pixels with an integration of 0.6 ms/pixel.

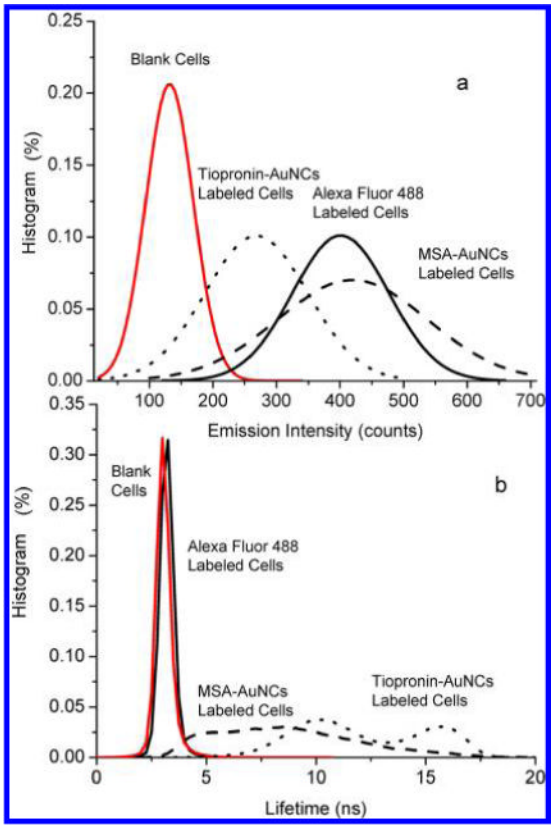

Figure 7.

Histogram distributions of (a) emission intensity and (b) lifetimes over the entire cell images that are loaded by PEGylated MSA-AuNCs and tiopronin-AuNCs. Histogram distributions of emission intensity and lifetimes throughout the entire cell images that were unlabeled or labeled by Alexa Fluor 488 dyes were also presented as references.